# Grating Lobe Reduction in Scanning Phased Array Antennas With Large Element Spacing

Zabed Iqbal, Student Member, IEEE, and Maria Pour<sup>®</sup>, Senior Member, IEEE

Abstract—Large element spacing in phased array antennas generally causes grating lobes, which start to exacerbate for wide scan angles. Herein, a new approach is proposed to reduce the grating lobes of planar phased array antennas with considerably large element spacing in the order of one wavelength for both broadside and scanned radiation patterns up to 45°. The array has a seven-element hexagonal configuration, consisting of dualmode circular microstrip antennas. It is shown that for small scan angles up to  $8^{\circ}$ , a tapered amplitude distribution reduces the grating lobes to below  $-30 \, dB$ , when only the dominant mode is excited in the antenna element. As for wider scan angles up to 45°, an additional higher order mode needs to be excited as well to reduce the grating lobes down to -30 dB for the large element spacing of one wavelength. The proposed method also proves to be effective for wider scan angles up to 60° for element spacing of three quarters of a wavelength. This approach leads to the realization of thinned arrays with less number of elements, in which the weighting functions and mode excitation of the elements can be controlled by an adaptive signal processing unit in scanning phased array antennas.

*Index Terms*—Element spacing, grating lobes, higher order modes, microstrip patch, phased arrays.

### I. INTRODUCTION

VER the last few years, phased array antennas with wide-angle scanning capabilities have attracted many researchers due to their widespread usage and high demand in different applications such as radar, direction finding, air traffic surveillance, microwave remote sensing, and weather forecast. In the aforementioned applications, where high-gain scanning antennas are required, it is common to use phased array antennas with large element spacing [1]. However, it generates grating lobes, which worsen for wide scan angles. Grating lobes reduce the aperture efficiency [1], [2] and directivity, which eventually degrade the overall antenna performance. Many methods have been proposed to address the grating lobe problems. For example, the odd-mode scanning technique using large aperture elements [3], [4], nonuniform element separation [5], array element shaping [6], and amplitude tapering at the subarray port including the randomization of

Manuscript received February 17, 2018; revised August 23, 2018; accepted September 30, 2018. Date of publication October 9, 2018; date of current version November 30, 2018. This work was supported in part by the National Science Foundation CAREER under Award ECCS-1653915. (Corresponding author: Maria Pour.)

The authors are with the Department of Electrical and Computer Engineering, The University of Alabama in Huntsville, Huntsville, AL 35899 USA (e-mail: zi0003@uah.edu; maria.pour@uah.edu).

Color versions of one or more of the figures in this paper are available online at http://ieeexplore.ieee.org.

Digital Object Identifier 10.1109/TAP.2018.2874717

subarray and row distribution [7] methods has been developed to reduce the grating lobes in phased array antennas with limited scan coverage.

Wide scan phased array antennas are required in the target tracking and direction finding applications, especially for the low elevation targets. Therefore, to retain low grating lobes for wider scan angles, a judicious selection of the element and interelement separation is needed. To this end, different optimization methods such as the genetic algorithm [8], [9] have been developed. Other methods include the use of leaky wave phased arrays [10] and mode matching techniques [11]. The aforementioned methods for grating lobe suppression were reported for nonplanar antenna elements with bulky structures. In emerging wireless applications, planar phased array antennas with printed elements have significant advantages. However, their scanning coverage is quite narrow, and the associated gain fluctuation is in the order of 4-5 dB [12]. In order to widen the scanned angle of such printed phased array antennas, pattern reconfigurability methods [13]–[16] and magnetic-electric dipole [17], [18] antennas have been used with element spacing around half a wavelength. A circular phased array consisting of dual-mode elements was reported in [19], where both the number of elements and grating lobes were reduced. However, its corresponding scanned angle was only about 8.5° off the boresight direction.

In this paper, a new approach is proposed to reduce the grating lobes of a microstrip patch antenna array with considerably large element spacing in the order of one wavelength for both broadside and scanned radiation patterns up to 45°. The array has a seven-element hexagonal configuration, comprising of a central element and six peripheral elements equally spaced on a circle. Each element is a dual-mode circular microstrip patch antenna, capable of exciting TM<sub>11</sub> and TM<sub>21</sub> modes. For broadside patterns and small scan angles up to 8°, only TM<sub>11</sub> mode needs to be excited, and the grating lobe reduction is realized by controlling the amplitude distribution of the peripheral elements of the phased array antenna. Later, it will be shown that the tapered amplitude distribution is no longer sufficient to suppress the grating lobes for wider scan angles. Thus, to effectively reduce the grating lobes, the higher order mode TM<sub>21</sub> is excited along with TM<sub>11</sub> mode in the microstrip patch antenna elements. For the element spacing of one wavelength, the grating lobes are reduced to well below -30 dB for a scan angle up to  $45^{\circ}$  by controlling the excitation ratio of TM<sub>11</sub> and TM<sub>21</sub> modes, as well as the array amplitude distribution. The proposed approach will also be examined for wider scan angles up to 60°, for element spacing of three

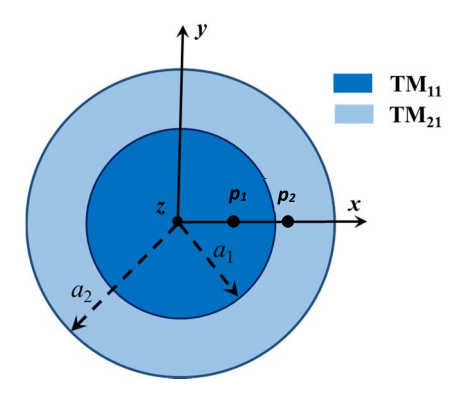


Fig. 1. Top view of a stacked circular microstrip patch antenna operating at  $TM_{11}$  and  $TM_{21}$  modes, where  $a_1$  and  $a_2$  are the radii of these modes, respectively;  $p_1$  and  $p_2$  represent probe locations along the *x*-axis.

quarters of a wavelength, resulting in at least -22 dB grating lobe reduction, which is promising for such wide scan angles.

### II. FORMULATION OF ANTENNA ELEMENT

The constitutive elements of the proposed phased array antenna, which is a seven-element hexagonal array with a triangular lattice, are dual-mode circular microstrip patch antennas, capable of exciting TM<sub>11</sub> and TM<sub>21</sub> modes at the frequency of 10 GHz. As it is known, the circular microstrip patch antenna produces broadside and conical radiation patterns while operating at the fundamental TM<sub>11</sub> mode and the higher order TM<sub>21</sub> mode, respectively [20]. When these two modes are simultaneously excited by a proper mode content factor, self-scanning antenna elements are realized that can be used as radiation-matched elements in scanning phased array antennas. To design such dual-mode antenna elements, one- and two-layer configurations may be used. The top view of the latter, i.e., a stacked configuration, is illustrated in Fig. 1, where  $TM_{11}$  and  $TM_{21}$  patches are placed on the top and middle layers, respectively, both supported by an infinite ground plane.

Based on the cavity model, assuming that the patch is supported by an infinite ground plane, the combined far-field radiation pattern equations for the x-polarized  $TM_{11}$  and  $TM_{21}$  modes can be written as [21]

$$\begin{split} E_{\theta} &= -j ([J_{0}(u_{1}) - J_{2}(u_{1})] cos\phi \\ &+ j A_{21} [J_{1}(u_{2}) - J_{3}(u_{2})] cos2\phi) \\ &= F_{11}(\theta) cos\phi + A_{21} F_{21}(\theta) cos2\phi \\ E_{\phi} &= j ([J_{0}(u_{1}) + J_{2}(u_{1})] sin\phi \\ &+ j A_{21} [J_{1}(u_{2}) + J_{3}(u_{2})] sin2\phi) cos\theta \\ &= -G_{11}(\theta) sin\phi - A_{21} G_{21}(\theta) sin2\phi \end{split} \tag{2}$$

where  $F_{nm}$  and  $G_{nm}$  are the radiation functions of the respective  $TM_{nm}$  modes. Here,  $u_1$  and  $u_2$  are defined by

$$\begin{cases} u_1 = k_o a_1 \sin \theta \\ u_2 = k_o a_2 \sin \theta \end{cases}$$
 (3)

where  $k_o$  is the wavenumber and  $a_1$  and  $a_2$  are the radii of TM<sub>11</sub> and TM<sub>21</sub> patches, respectively.  $A_{21}$  is the normalized

excitation ratio of TM<sub>21</sub>-to-TM<sub>11</sub> modes and is a complex number in the form of  $A_{21} = |A_{21}| \angle \alpha_{21}$ , where  $\alpha_{21}$  is the phase shift between the two modes.  $J_m(u)$  is the Bessel function of the first kind of order m, where m changes from 0 to 3. The zeros of the derivatives of the Bessel function determine the order of the resonant frequencies and the effective radii of the patches. For TM<sub>11</sub> and TM<sub>21</sub> modes, the associated eigenvalues are 1.8412 and 3.0542, respectively. For simplicity, the supporting dielectric substrate is selected as air with a height of 1.6 mm. Thus, the physical radii for  $TM_{11}$  and  $TM_{21}$  modes are  $a_1 = 7.3$  mm and  $a_2 = 12.8$  mm, respectively, at the selected frequency of 10 GHz. The probe feeds exciting  $TM_{11}$  and  $TM_{21}$  modes, denoted by  $p_1$  and  $p_2$ in Fig. 1, respectively, are positioned along the x-axis. As it will be shown later, either a single-mode TM<sub>11</sub> or a dualmode antenna element will be used in the array for small and wide scan angles, respectively. Therefore, the direction of the array polarization is mainly dependent on that of TM<sub>11</sub> mode, which is x-polarized as per (1) and (2). The corresponding co-pol component of the element pattern can be expressed using Ludwig's third definition [22] as

$$E_{co} = F_{11}(\theta) \cos^2 \phi + G_{11}(\theta) \sin^2 \phi + A_{21}[F_{21}(\theta) \cos 2\phi \cos \phi + G_{21}(\theta) \sin 2\phi \sin \phi].$$
 (4)

Thus, the co-pol component at the principal planes is given by

$$\begin{cases} E_{co}|_{\phi=0^{\circ}} = F_{11}(\theta) + A_{21}F_{21}(\theta) \\ E_{co}|_{\phi=90^{\circ}} = G_{11}(\theta). \end{cases}$$
 (5)

The total co-pol component of the array will be the product of (4) and the array factor. Therefore, the polarization of the array remains stable for both on- and off-boresight scan angles and is parallel to the *x*-axis.

### III. ANTENNA ELEMENT RADIATION PATTERN

The analytical model of the antenna element presented in Section II has been further studied, and the results of a single-element dual-mode circular microstrip patch antenna will be presented in this section. Fig. 2 depicts the normalized radiation patterns of the single-element circular microstrip antenna operating at the individual  $TM_{11}$  and  $TM_{21}$  modes. As it can be seen, the microstrip patch antenna excited at TM<sub>11</sub> mode generates broadside radiation patterns, as shown in Fig. 2(a). The radiation pattern of the  $E_{\theta}$  component at the  $\phi = 0^{\circ}$  plane is broader than that of the  $E_{\phi}$  component at the  $\phi = 90^{\circ}$  plane. As for TM<sub>21</sub> mode, the radiation patterns become conical with a null at the boresight direction of  $\theta = 0^{\circ}$ , as shown in Fig. 2(b). The peak of the normalized radiation patterns of TM<sub>21</sub> mode is around  $\pm 35^{\circ}$  for both  $E_{\theta}$  and  $E_{\phi}$ components at the elevation plane. A similar trend in terms of beamwidths is observed for  $TM_{21}$  mode. That is, the  $E_{\theta}$ component at the  $\phi=0^\circ$  plane is slightly broader than that of the  $E_{\phi}$  component at the  $\phi = 45^{\circ}$  plane. These are expected, as an infinite ground plane is assumed for both modes.

In order to examine the effect of the higher order mode on the element pattern and the scanning capabilities of the dual-mode patch, different mode content factors, or commonly known as excitation ratios, have been studied by changing both

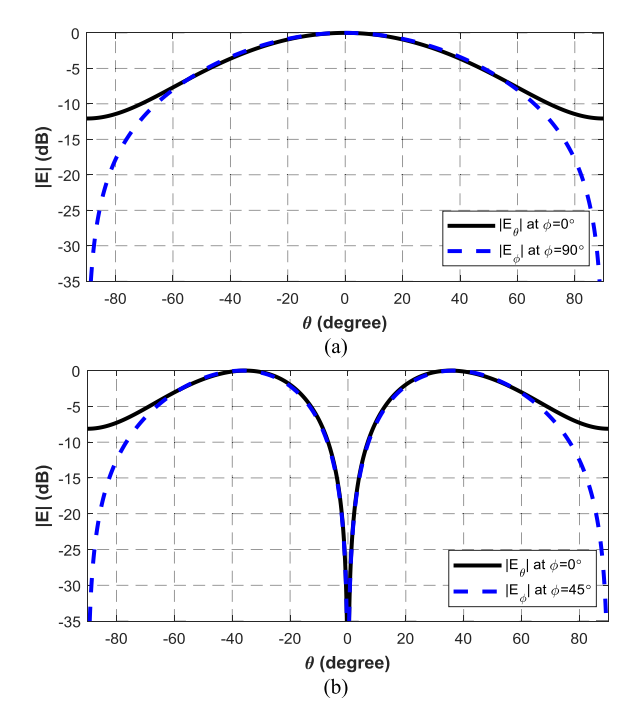


Fig. 2. Normalized radiation patterns of a circular microstrip patch antenna operating at (a)  $TM_{11}$  mode (b)  $TM_{21}$  mode.

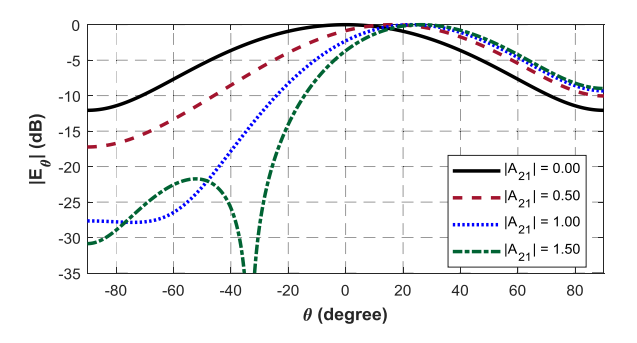


Fig. 3. Normalized radiation patterns of  $E_{\theta}$  of a single-element patch with combined  $TM_{11}$  and  $TM_{21}$  modes at the  $\phi=0^{\circ}$  plane for different magnitude excitation ratios  $|A_{21}|$ , when  $\alpha_{21}=-90^{\circ}$ .

magnitude excitation, i.e.,  $|A_{21}|$ , and phase shifts between the modes, i.e.,  $\alpha_{21}$ . At the  $\phi=0^\circ$  plane, the  $E_\theta$  component is the contribution of both TM<sub>11</sub> and TM<sub>21</sub> modes, while the  $E_\phi$  component becomes 0 as per (1) and (2). Therefore, only  $E_\theta$  radiation patterns are presented in this paper. The results for different magnitude excitation ratios with a quadrature phase shift of  $-90^\circ$  are plotted in Fig. 3. For the constant phase shift of  $\alpha_{21}=-90^\circ$ , the radiation pattern tends to transform from broadside to scanned patterns, as the magnitude excitation ratios increase. In the limit, when the magnitude excitation is much greater than unity, i.e.,  $|A_{21}| \gg 1$ , the contribution of TM<sub>11</sub> mode will be negligible, and the radiation patterns eventually approach to those of the pure TM<sub>21</sub> mode.

When the phase shift  $\alpha_{21}$  between the two modes under study varies from  $0^{\circ}$  to  $-90^{\circ}$ , the main beam is scanned toward positive elevation angles with the increase of the magnitude excitation ratios. It is worth mentioning that the main beam of the single-element dual-mode antenna symmetrically scans to

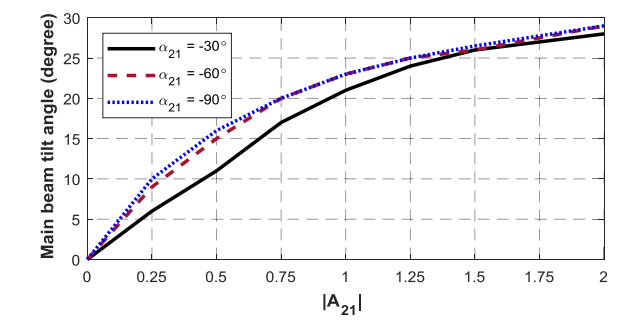


Fig. 4. Effects of magnitude excitation ratio of  $|A_{21}|$  on the main beam tilt angle of a single-element patch with combined  $TM_{11}$  and  $TM_{21}$  modes at the  $\phi = 0^{\circ}$  plane for a different  $\alpha_{21}$ .

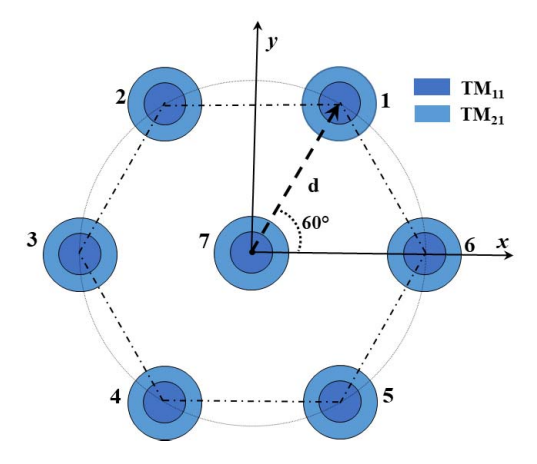


Fig. 5. Geometry of the hexagonal seven-element antenna array consisting of dual-mode circular patch elements; six elements are placed along a circle and one element in the center with element spacing d.

the negative direction, if positive phase shifts are applied to the two modes. Fig. 4 shows the main beam scan angles, at the element level, against mode excitation ratios for three selected phase shifts of  $-30^{\circ}$ ,  $-60^{\circ}$ , and  $-90^{\circ}$ . It should be noted that the main beam does not scan off the broadside direction for the in-phase excitation of  $\alpha_{21} = 0^{\circ}$  until the magnitude excitation ratio becomes much greater than unity, i.e.,  $|A_{21}| \gg 1$ , which then results in conical radiation patterns with split main beams, since the dominating mode will be TM<sub>21</sub> mode. As shown in Fig. 4, to obtain a maximum scanned angle for the dualmode circular patch antennas, the phase shifts between the two modes should be  $\pm 90^{\circ}$ , for a given  $|A_{21}|$ . Therefore, to fully utilize the potential of such self-scanning antenna elements in the proposed phased array under investigation, the two modes will be excited with the 90° quadrature phase shift, where applicable.

### IV. FORMULATION OF ARRAY FACTOR

The proposed scanning phased array is a seven-element hexagonal array, consisting of one central element surrounded by six peripheral elements, as shown in Fig. 5. The peripheral elements are distributed evenly over a circle of radius d with an angular separation of  $60^{\circ}$ . The antenna elements are the dual-mode circular patch antennas that are defined by (1) and (2).

The array factor of the seven-element hexagonal array under investigation is expressed by

$$AF(\theta,\phi) = 1 + \sum_{n=1}^{6} w_n e^{j(kdsin\theta cos(\phi - \phi_n) + \beta_n)}$$
 (6)

where  $w_n$  is the amplitude distribution of the six peripheral elements and  $\phi_n$  is the angular position of the *n*th element located on the circle. Both are given by

$$\phi_n = \frac{\pi n}{3} \tag{7}$$

$$w_n = \begin{cases} 1, & n = 0 \\ w, & n \neq 0 \end{cases} \text{ where } 0.1 < w < 1.$$
 (8)

For simplicity, it is assumed that the amplitude distribution of the peripheral elements is normalized to that of the central one. That is,  $w_n$  is equal to unity for the central element and it varies from 0.1 to 1 for the six peripheral elements.

To scan the main beam to an angle of  $(\theta_0, \phi_0)$ , a phase term is added with each element of the array. The phase term of the *n*th element is, thus, expressed by

$$\beta_n = -kd \sin\theta_0 \cos(\phi_0 - \phi_n) \tag{9}$$

where  $\beta_n$  is the progressive phase shift of the *n*th peripheral element relative to the array center. Thus, the array factor is a function of the array geometry, phase excitation, and amplitude distribution  $w_n$  of the peripheral elements of the array. By varying the amplitude distribution  $w_n$ , element separation d, and/or phase excitation  $\beta_n$ , the characteristics of the array factor as well as the total electric field of the array can be obtained by simply multiplying the array factor, given by (6), and the element patterns governed by (1) and (2).

As an example, the simplified array factor for the broadside radiation pattern, where the peripheral elements are uniformly weighted by w, can be written as

$$AF(\theta,\phi) = 1 + w \left[ 2\cos X + 4\cos\left(\frac{1}{2}X\right)\cos\left(\frac{\sqrt{3}}{2}Y\right) \right]$$
(10)

where

$$X = kd \sin\theta \cos\phi$$
  

$$Y = kd \sin\theta \sin\phi.$$
 (11)

### V. ARRAY RADIATION PATTERN FOR ONE-WAVELENGTH ELEMENT SPACING

In this section, a planar scanning phased array antenna with large element spacing of one wavelength is investigated in order to reduce its unwanted grating lobes. As shown in Fig. 5, the array is comprised of a total seven elements, where one element is located in the center and the other six elements are evenly distributed over a circle of one-wavelength radius. Each element is a dual-mode microstrip patch antenna, capable of generating broadside and boresight-null radiation patterns by exciting  $TM_{11}$  and  $TM_{21}$  modes, respectively.

As it is well known, one of the limiting factors for grating lobe reduction in scanning phased array antennas is the

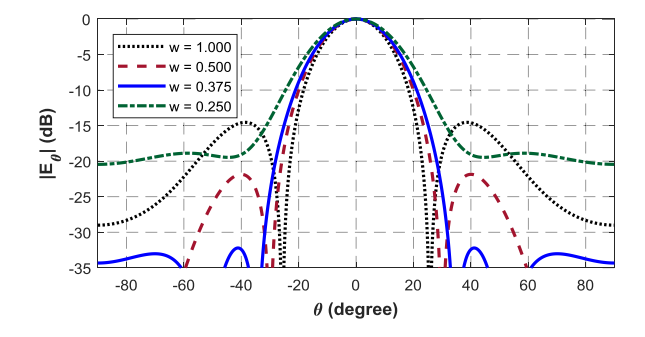


Fig. 6. Normalized radiation patterns of the seven-element phased array antenna shown in Fig. 5, when each element operates at  $TM_{11}$  mode for different amplitude distributions w of peripheral elements with  $d = \lambda$ .

element spacing. The maximum element spacing of a linear array with a rectangular lattice to avoid grating lobes for a scan angle of  $\theta_0$  may be written as [12]

$$d_{max} = \frac{\lambda}{1 + |\cos\theta_0|}. (12)$$

As an example, for a scan angle of  $45^{\circ}$ , the maximum allowable element spacing according to (12) is  $0.586\lambda$ . Therefore, the realization of arrays with larger element spacing and reduced grating lobes becomes quite challenging, which is the main objective of this paper. In this paper, much larger element spacing in the order of  $\lambda$  is considered for the planar array to show how the addition of higher order modes along with tapered amplitude distributions of the peripheral elements can effectively reduce the grating lobes. Since the element spacing is considered in the order of  $\lambda$ , the total electric field is computed assuming that the mutual couplings between array elements are negligible. The results of different scan angles, when  $d = \lambda$ , will be shown in Sections V-A and V-B.

### A. Results for Scan Angles Up to $8^{\circ}$ With $d = \lambda$

It is found that only  $TM_{11}$  mode needs to be excited in the antenna element for broadside patterns and small scan angles up to  $8^{\circ}$ . Interestingly enough, it has been observed that the unwanted grating lobes can be effectively reduced by tapering the amplitude distribution of the peripheral elements. To this end, the amplitude distribution of the central element is kept unity, while that of the peripheral elements, i.e., w in (6), is tapered to decimal numbers. As expected, the grating lobe level decreases up to a certain value. In the simplest case of broadside radiation, when w is further reduced below 0.37 for the  $\lambda$  element spacing, the grating lobe level starts to rise again, as shown in Fig. 6. This is due to the fact that such a tapered distribution approximates the Gaussian distribution, where the sidelobes eventually merge with the main lobe.

For the broadside case, the normalized radiation patterns of the seven-element planar phased array are depicted in Fig. 6 when each antenna element supports only TM<sub>11</sub> mode. Several radiation patterns are plotted and compared for different values of w, including 0.25, 0.375, 0.5, and 1. As it is observed, the grating lobes as low as -32.4 dB are obtained, when w = 0.375. This is remarkable in comparison with the uniform amplitude excitation case, i.e., w = 1, when the grating lobe is quite high around -15 dB. As per

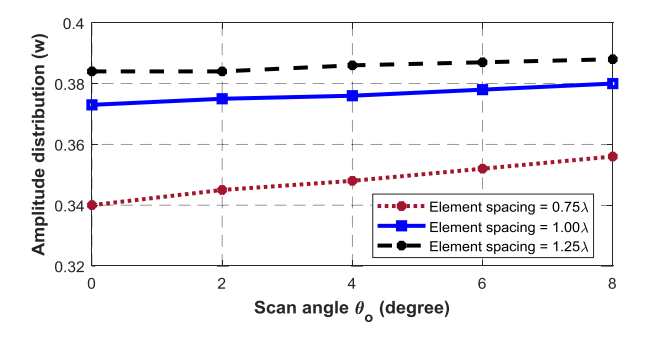


Fig. 7. Finalized values of the amplitude distribution w of the six peripheral elements against scan angles up to  $8^{\circ}$  for different element spacings, when the elements are single-mode  $TM_{11}$  patches to reduce the grating lobes to below -30 dB.

Fig. 6, any tapered distribution will reduce the grating lobe to below -15 dB; however, it tends to merge with the main beam for w as small as 0.25. Another finer search routine was performed around w = 0.375, to ensure it yields the best possible grating lobe reduction for the element spacing of one wavelength. The associated results are omitted here for brevity.

After extensive study, it is found that for small scan angles up to 8°, the grating lobes can be easily reduced to well below -30 dB by controlling the amplitude distribution of the peripheral elements only when the antenna elements support the single-mode  $TM_{11}$ . This is expected, as any tapered excitation will lower the sidelobe levels (SLLs). In addition, the radiation pattern of the antenna element, which is now broadside, almost matches to that of the array factor. Fig. 7 shows the optimized values of the amplitude distribution w for the scan angle from 0° to 8°, to reduce the grating lobe levels to well below -30 dB, for three different element spacings of  $0.75\lambda$ ,  $\lambda$ , and  $1.25\lambda$ . As it can be seen, the larger the element spacing, the greater is w. The average optimum values of w are around 0.35, 0.375, and 0.385, for the abovementioned element spacing, respectively. If the main beam is scanned beyond the direction  $\theta_0 = 8^{\circ}$ , the grating lobe level further rises, which necessitates the excitation of the next higher order TM<sub>21</sub> mode in addition to  $TM_{11}$  mode at the element level. Consequently, dual-mode antenna elements, supporting both TM<sub>11</sub> and TM<sub>21</sub> modes, will better facilitate reducing the grating lobes. This is due to the fact that such self-scanning antenna elements, as per Fig. 3, can partially nullify the grating lobes even for large element spacing. The corresponding results will be presented in Sections V-B and VI.

### B. Results for Scan Angle From $8^{\circ}$ to $45^{\circ}$ With $d = \lambda$

As mentioned earlier, to effectively reduce the grating lobes for medium scan angles from  $8^{\circ}$  to  $45^{\circ}$ , herein, dual-mode microstrip antenna elements, capable of simultaneously exciting both  $TM_{11}$  and  $TM_{21}$  modes, are investigated. The idea is to partially nullify the grating lobes occurring in the vicinity of the element null position. The element spacing of one wavelength is assumed. The total radiation patterns of the hexagonal array under study are shown in Figs. 8–10, for the scan angles of  $20^{\circ}$ ,  $30^{\circ}$ , and  $40^{\circ}$ , respectively. To shed light on the proposed technique, Figs. 8–10 include the

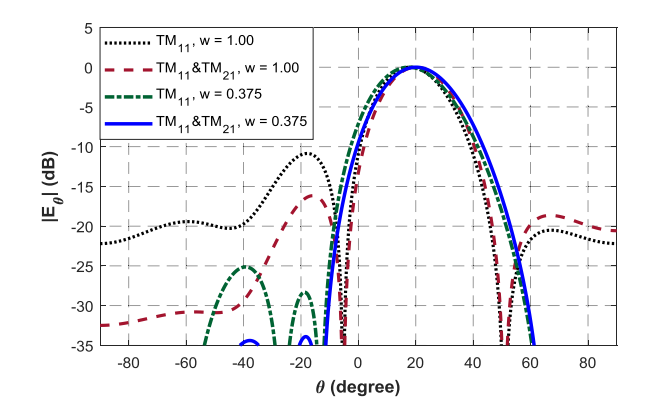


Fig. 8. Normalized radiation patterns of the seven-element phased array antenna shown in Fig. 5 with  $d = \lambda$  and a scan angle of 20°, with both single-and dual-mode antenna elements, excited by uniform and tapered amplitude distributions; for the dual-mode case:  $A_{21} = 0.75 \angle -90^{\circ}$ .

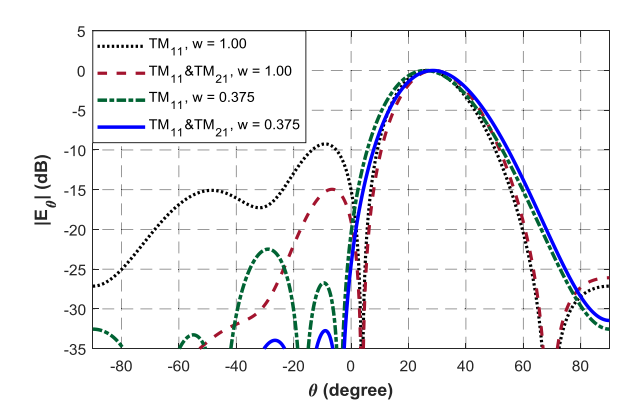


Fig. 9. Normalized radiation patterns of the seven-element phased array antenna shown in Fig. 5 with  $d=\lambda$  and a scan angle of 30°, with both single-and dual-mode antenna elements, excited by uniform and tapered amplitude distributions; for the dual-mode case:  $A_{21}=1.0 \angle -90^\circ$ .

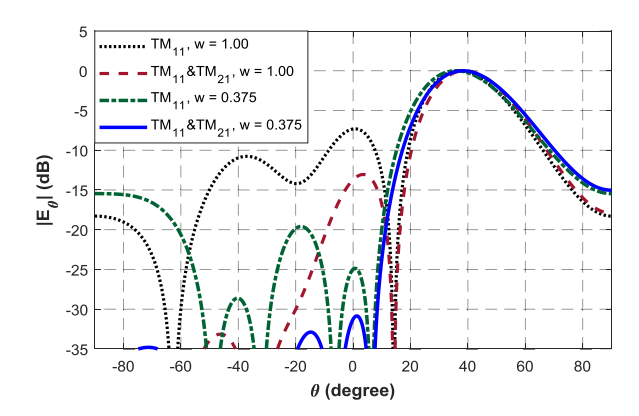


Fig. 10. Normalized radiation patterns of the seven-element phased array antenna shown in Fig. 5 with  $d=\lambda$  and a scan angle of 40°, with both single-and dual-mode antenna elements, excited by uniform and tapered amplitude distributions; for the dual-mode case:  $A_{21} = 1.50 \angle -90^{\circ}$ .

associated patterns of single- and dual-mode antenna elements, with uniform and tapered distributions. The reference case is the hexagonal array consisting of single-mode  $TM_{11}$  antenna elements, which are uniformly excited with w=1. As it is observed, the corresponding grating lobes for this reference case are quite high, and they change from -11 to -7 dB, as the

TABLE I
FINALIZED VALUES OF THE EXCITATION RATIOS AND TILT ANGLES
OF THE MATCHED ELEMENTS WHEN AMPLITUDE DISTRIBUTION
IS 0.375 AND ELEMENT SPACING IS ONE WAVELENGTH

Scan angle $(\theta_0)$	Amplitude excitation ratio $( A_{2l} )$	Phase excitation ratio $(\alpha_{21})$	Max tilt angle of the element
0°-8°	0	NA	0°
10°	0.25	-90°	10°
20°	0.75	-90°	20°
30°	1.00	-90°	23°
40°	1.50	-90°	26°
45°	2.00	-90°	29°

main beam is scanned from 20° to 40°. Although the tapered single-mode cases, where w equals 0.375, lower the SLLs, they fail to reduce the second minor or far-out lobes, as illustrated in Figs. 8–10. As for the dual-mode cases, grating lobes are reduced and -30 dB, or lower sidelobes are realized when the array is excited by nonuniform amplitude distributions. To the best of our knowledge, such a significant reduction is unprecedented for medium scan angle arrays with  $d = \lambda$ . After extensive study, it turns out that the optimum value of w is 0.375, which is close to the value that was found for the small scan angles, when  $d = \lambda$ , in Section V-A. The important factor to enable such grating lobe reduction is the judicious selection of the mode content factors at the element level to provide the radiation-matched elements for a given scan angle. This is crucial as it controls the main beam of the element pattern and its null position, as per Fig. 3. For the selected medium scan angles of 20°, 30°, and 40°, the mode content factors of the dual-mode antenna elements are found as 0.75, 1, and 1.5, respectively, along with a  $-90^{\circ}$  phase shift between the two modes.

For the element spacing of one wavelength and w=0.375, the required mode content factors for low and medium scan angles up to  $45^{\circ}$  are listed in Table I to reduce the grating lobes to below -30 dB. Moreover, information on the self-scanning properties of such dual-mode antenna elements is included in Table I. For example, for a scan angle of  $\theta_0=45^{\circ}$ , the main beam of the radiation-matched element is tilted to  $29^{\circ}$ , and the required mode excitation is 2 with a  $-90^{\circ}$  phase shift. Table I may serve as lookup data in the signal processing unit for reducing the grating lobes over the course of the array operation for a given scan angle.

For the hexagonal array under investigation, it is instructive to examine the grating lobe reduction at other azimuth planes, especially up to 30°, in addition to the  $\phi=0^\circ$  plane shown thus far. The corresponding array factor with w=0.375 is plotted in Fig. 11(a), when the element spacing is one wavelength and the scan angle is 30°. As it can be seen, all the array factors at the  $\phi=5^\circ$ , 15°, and 25° planes have grating lobes greater than -11 dB. Fig. 11(b) shows the total radiation patterns of the array with the proposed dual-mode elements at different azimuth planes of  $\phi=5^\circ$ , 15°, and 25° for the same scan angle of  $\theta_0=30^\circ$  and w=0.375. The grating lobes have reduced to well below -26 dB at these  $\phi$ -cut planes. This is quite remarkable compared with the reference case

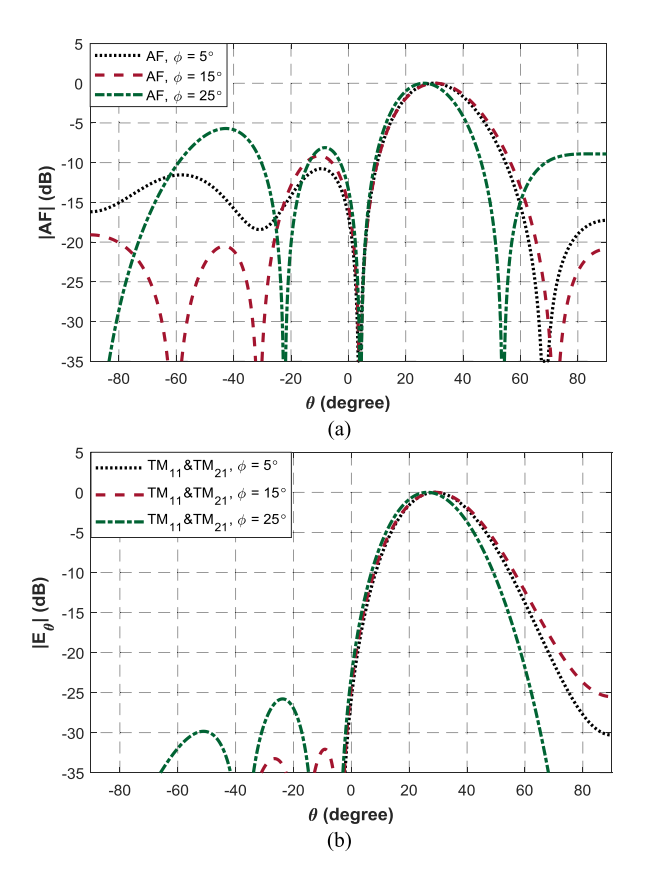


Fig. 11. (a) Normalized array factor and (b) total radiation patterns of the seven-element array in Fig. 5 with  $d=\lambda$  and a scan angle of  $\theta_0=30^\circ$  at different azimuth planes, when w=0.375; for total radiation patterns, the elements are the dual-mode patches with  $A_{21}=1.0\angle-90^\circ$ .

shown in Fig. 9, where only TM<sub>11</sub> mode was excited with a uniform amplitude distribution, i.e., w = 1, exhibiting a grating lobe as high as -9 dB. For the total radiation patterns shown in Fig. 11(b), the mode content factors of the dual-mode antenna elements are  $|A_{21}| = 1$  and  $\alpha_{21} = -90^{\circ}$ .

To further demonstrate the effectiveness of the proposed grating lobe suppression technique, the hexagonal array of the dual-mode elements has been compared with conventional linear arrays, including Dolph–Tschebyscheff array of -30 dB SLL, binomial array, and a linear array with an amplitude taper of w=0.375, with the same element spacing of one wavelength. The results are plotted in Fig. 12 for a scan angle of  $\theta_0=30^\circ$ . Each of the aforementioned linear arrays is a seven-element array consisting of  $TM_{11}$  circular patch antennas. As can be seen from Fig. 12, in the conventional amplitude taper arrays, the grating lobes are still high and in the same level as the main beam in the opposite direction; whereas with the proposed method, the grating lobe is significantly suppressed by utilizing the nulling and self-scanning properties of the dual-mode circular patch as described in Section III.

Table II provides a comprehensive comparison among the proposed method and some previously reported methods on grating lobe reduction. As it can be seen, the proposed dual-mode hexagonal array outperforms other methods in terms of grating lobe reduction, scan coverage, and element spacing. Moreover, the proposed method utilizes a planar 2-D

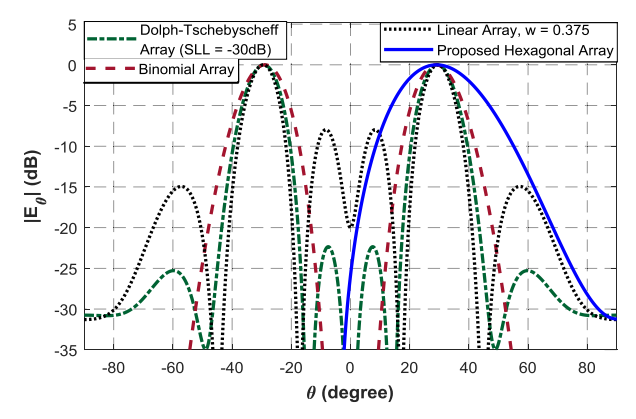


Fig. 12. Comparison of the grating lobe suppression capability of the proposed hexagonal phased array using dual-mode antenna elements with the conventional amplitude taper in seven-element linear arrays with single-mode elements, when  $d=\lambda$ .

TABLE II

COMPARISON OF GRATING LOBE REDUCTION, MAXIMUM SCAN ANGLE,
AND ELEMENT SPACING OF THE PROPOSED METHOD WITH
PREVIOUSLY REPORTED METHODS

Ref []	Element type	Grating	Max. Scan	Element
		Lobe Level	Angle	Spacing
[3]	Horn Antenna	-13 dB	10°	1.7λ
[4]	Horn Antenna	-20 dB	10.3°	1.0 λ
[7]	Point Source	-20 dB	45°	0.5λ
[9]	Dipole Antenna	-10 dB	60°	0.8λ
[10]	Leaky-Wave Antenna	-10 dB	8.6°	1.5λ
[16]	Square Loop Antenna	-10 dB	60°	0.9λ
[17]	Microstrip Mag. Dipole	-4.8 dB	70°	0.4λ
[18]	Magelectric Dipole	-10.2 dB	66°	0.48λ
This	Circular Dual-Mode	<-30 dB	Up to 45°	1.0 λ
work	Microstrip Patch	<-22 dB	Up to 60°	0.75 λ

configuration, as a single- or stacked-layer circular microstrip patch antenna can be used as an array element, which is preferred over nonplanar antenna elements with bulky structures.

To complete our investigation on small and medium scan angles, a sequence of normalized radiation patterns, as well as the corresponding cross-pol components at the diagonal plane of  $\phi=45^\circ$ , of the seven-element phased array antenna with axial and scanned main beams are plotted in Fig. 13, starting from  $\theta_0=0^\circ$  to  $\theta_0=40^\circ$ , when  $d=\lambda$ . All the grating lobes of the total radiation patterns, i.e., the product of the antenna element and the array factor, have been reduced to well below -30 dB. The cross-pol components in the worst case scenario are lower than -15 dB. For the broadside and small scan angle up to  $8^\circ$ , only TM<sub>11</sub> mode is excited, whereas for the scanning angle from  $\theta_0=10^\circ$  to  $\theta_0=45^\circ$ , both TM<sub>11</sub> and TM<sub>21</sub> modes are excited.

### VI. ARRAY RADIATION PATTERN FOR 0.75-WAVELENGTH ELEMENT SPACING

Thus far, most of the presented results of the hexagonal seven-element phased array are numerically computed by considering the element spacing as  $d = \lambda$ . In this section, the proposed method of grating lobe reduction will further

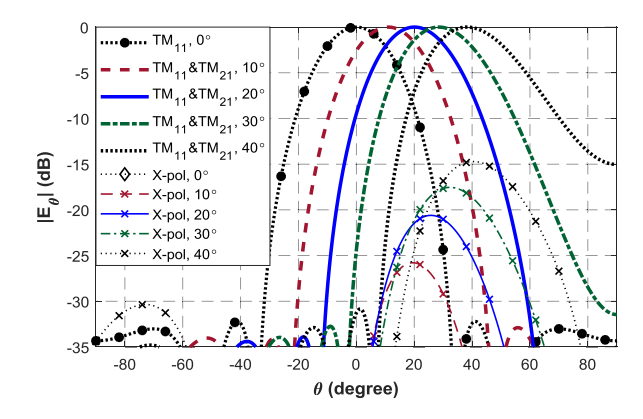


Fig. 13. Normalized radiation patterns with reduced grating lobes and cross-pol patterns at the  $\phi=45^\circ$  plane of the seven-element phased array antenna shown in Fig. 5 with  $d=\lambda$ , as the main beam scans from  $0^\circ$  to  $40^\circ$ ; the elements are single-mode  $TM_{11}$  patches for the broadside pattern and  $TM_{11}+TM_{21}$  mode patches for  $10^\circ-40^\circ$  scan angles.

be examined numerically for wider scan angles, such as  $50^{\circ}$  and  $60^{\circ}$ , with slightly smaller element spacing of  $0.75\lambda$ to explore its potential in the grating lobe reduction. For consistency, both uniform and tapered amplitude distributions are investigated, corresponding to w = 1 and w = 0.375, respectively. The results are shown in Fig. 14(a) and (b), for scan angles of 50° and 60°, respectively. As per Fig. 14, the grating lobes are lowered to -29 and -22.5 dB, when the dual-mode antenna elements are utilized in the array with the nonuniform amplitude distribution of w = 0.375, for scan angles of 50° and 60°, respectively. This is still significant compared with the results reported in the literature for such wide-angle scanned arrays with the element spacing of three quarters of a wavelength. The corresponding crosspol components at the diagonal plane are below -12.5 dB, for both 50° and 60° scan angles.

Therefore, to reduce the grating lobes in a microstrip patch array antenna with element spacing in the order of one wavelength, one needs to excite an additional higher order mode, especially for scan angles greater than  $8^{\circ}$ . In this paper,  $TM_{11}$  and  $TM_{21}$  modes are excited to reduce the grating lobe levels for scan angles up to  $60^{\circ}$ . Excitation of other higher order modes would further facilitate grating lobe reduction for even wider scan angles beyond  $60^{\circ}$ , which is currently being investigated by the authors and will be reported in the near future. For better clarification, Fig. 15 illustrates the schematic of the effective region of the single-mode and multimode elements for each of the low, medium, and wide scan coverages to reduce the grating lobes below -30 dB in the seven-element microstrip patch phased array antenna with element spacing of  $\lambda$ .

### VII. FULL-WAVE SIMULATION RESULTS

In Sections V and VI, analytical results based on the cavity model were presented for grating lobe reduction in a hexagonal array of dual-mode elements, in which mutual coupling between the elements was not taken into consideration. In general, errors due to mutual coupling, especially in wide-scanning arrays with small element spacing, can be

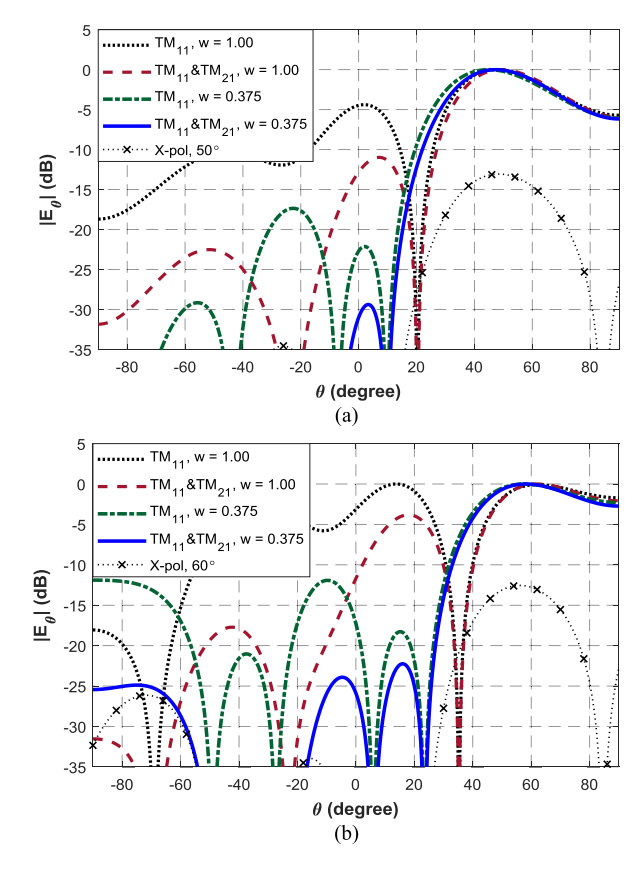


Fig. 14. Normalized radiation patterns and cross-pol patterns at the  $\phi=45^\circ$  plane of the seven-element phased array antenna shown in Fig. 5 with  $d=0.75\lambda$ , with both single- and dual-mode antennas, excited by uniform and tapered amplitude distributions, for scan angles of (a) 50° and (b) 60°; the dual-mode element is excited by  $A_{21}=2.0\angle-90^\circ$ .

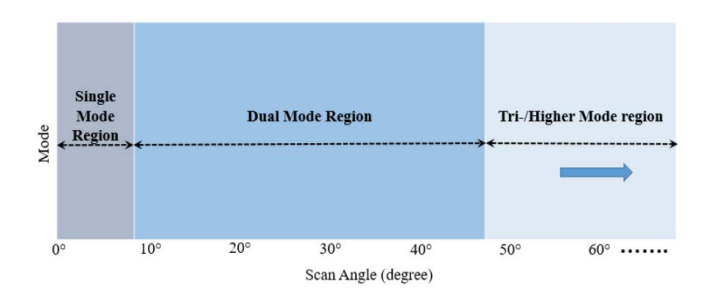


Fig. 15. Schematic of single-mode and multimode antenna elements for grating lobe reduction in hexagonal arrays with  $d = \lambda$ , low-, medium-, and wide-scan coverages.

significant and may degrade the array performance. In this section, to address the mutual coupling between the elements and edge effects, the proposed seven-element hexagonal array consisting of a stacked dual-mode circular patch antenna with one-wavelength element spacing is simulated using ANSYS HFSS [23], which is a finite-element-based full-wave electromagnetic solver. The stacked dual-mode antenna element, depicted in Fig. 1, is fed by two probes to individually excite TM<sub>11</sub> and TM<sub>21</sub> modes. The TM<sub>21</sub> patch is directly excited by a coaxial probe. As the electric field of TM<sub>21</sub> patch inside the cavity is 0 at its center, a shorting wall is placed at its center connected to the ground plane, through which the second probe is passed, connected to an L-probe to excite the top

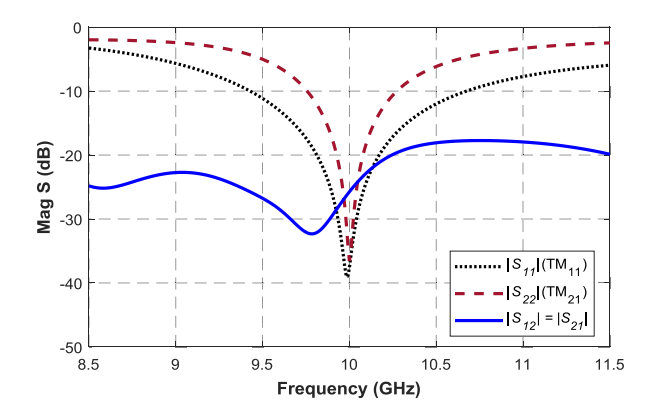


Fig. 16. Simulated scattering parameters of the dual-mode stacked patch antenna element shown in Fig. 1 operating at  $TM_{11}$  and  $TM_{21}$  modes over an infinite ground plane.

## TABLE III SIMULATED VALUES OF MUTUAL COUPLING BETWEEN THE ELEMENTS AT 10 GHz IN THE SEVEN-ELEMENT HEXAGONAL PHASED ARRAY ANTENNA WITH ONE-WAVELENGTH ELEMENT SPACING

Group	Mode	Element position	Coupling(dB)
1	$TM_{11} \longrightarrow TM_{11}$	All positions	<-30 dB
2	$TM_{11} \longrightarrow TM_{21}$	All positions	<-30 dB
3	$TM_{21} \longrightarrow TM_{21}$	Adjacent	<-20 dB
4	$TM_{21} \longrightarrow TM_{21}$	Non-adjacent	<-30 dB

layer, i.e.,  $TM_{11}$  patch. The simulated scattering parameters of the stacked dual-mode circular patch antenna are shown in Fig. 16, where  $S_{12}$  or  $S_{21}$  represents the mutual coupling between  $TM_{11}$  and  $TM_{21}$  modes in a single element, and  $S_{11}$  and  $S_{22}$  are the reflection coefficients of the ports exciting  $TM_{11}$  and  $TM_{21}$  modes, respectively. As it can be seen, the reflection coefficients are well below -10 dB within a frequency range of 9.45–10.7 and 9.75–10.25 GHz for  $TM_{11}$  and  $TM_{21}$  modes, respectively. They are below -35 dB at 10 GHz, providing excellent impedance matching at the frequency of operation. Interestingly enough, the mutual coupling of the stacked dual-mode element is around -25 dB at the frequency of 10 GHz, which is quite low.

The simulated scattering parameters of the seven-element hexagonal array under investigation are shown in Fig. 17, and a summary is also listed in Table III. In total, there are 14 ports in the array, two for each element to excite  $TM_{11}$  and  $TM_{21}$  modes. Thus, to simplify the results, the associated mutual coupling between the elements is classified into four groups as follows:

- 1) mutual coupling between TM<sub>11</sub> modes;
- 2) mutual coupling between TM<sub>11</sub> and TM<sub>21</sub> modes;
- 3) mutual coupling between TM<sub>21</sub> modes in adjacent
- 4) mutual coupling between  $TM_{21}$  modes in nonadjacent elements.

As per Fig. 17, the mutual coupling better than -30 dB is realized for all above groups, with the exception for group 3, where the coupling between two adjacent  $TM_{21}$  modes is around -20 dB, which is still low enough.

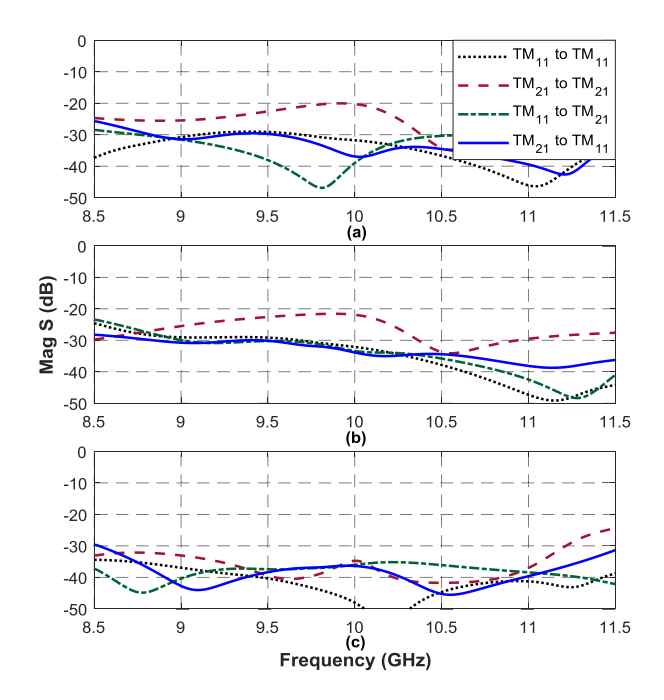


Fig. 17. Simulated scattering parameters representing mutual coupling between (a) center-to-edge and vice versa, (b) edge-to-edge (adjacent), and (c) edge-to-edge (nonadjacent) elements of the seven-element hexagonal phased array antenna with one-wavelength element spacing.

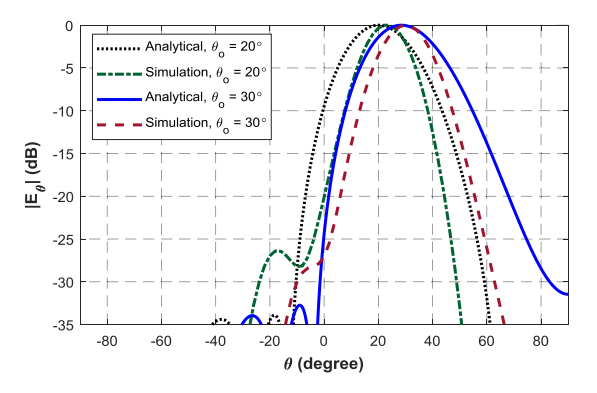


Fig. 18. Comparison of analytical and simulated radiation patterns of the seven-element array antenna in Fig. 5 with  $d=\lambda$  for scan angles of  $20^{\circ}$  and  $30^{\circ}$ .

To further examine the grating lobe reduction capability of the proposed method with the presence of mutual coupling, the full-wave simulation has been carried out by properly applying phase shifts among the elements, mode content factors, and tapered amplitude distribution of the peripheral elements, as per our analytical predictions. As representative examples, the corresponding results for the scan angles of 20° and 30° are shown in Fig. 18. Due to the moderate coupling between the adjacent TM<sub>21</sub> modes and probe effects, the amplitude distribution of peripheral elements, i.e., w is tuned to 0.35 instead of 0.375 of the analytical prediction, while mode content factors and phase shifts remain unchanged, as summarized in Table IV. The simulated grating lobe levels for the 20° and 30° scan angles are around -26.5 and -28.5 dB, respectively, whereas in the analytical study, they were below -30 dB for both cases. Nonetheless, such reduced grating lobes as low as -26.5 dB with the

#### TABLE IV

COMPARISON OF THE ANALYTICAL AND SIMULATED VALUES OF THE EXCITATION RATIOS AND AMPLITUDE DISTRIBUTION WHEN ELEMENT SPACING IS ONE WAVELENGTH

A 14.14m		Analytical		Full-wave Simulation	
<b>e</b>	$[A_{2i} \angle \alpha_{i}]$	w	G.L.* Level	w	G.L.* Level
20°	0.75∠-90°	0.375	<-30 dB	0.35	-26.5 dB
30°	1.00∠-90°	0.375	<-30 dB	0.35	-28.5 dB

\*G.L. stands for grating lobe

presence of mutual coupling is significant in scanning phased array antennas with one-wavelength element spacing. The discrepancy between the analytical and numerical results, observed in the radiation profile of each scan angle in Fig. 18, is mainly attributed to the probes, which were not included in the analytical approach based on the cavity model.

### VIII. CONCLUSION

A novel approach, based on tapered amplitude distributions and excitation of higher order modes, was proposed to reduce the grating lobes in a scanning phased array antenna with large element spacing in the order of one wavelength. The array consisted of circular microstrip patch antenna elements, forming a seven-element hexagonal configuration. It was shown that for axial beams and small scan angles up to 8°, single-mode patch elements were sufficient to reduce the grating lobes down to -30 dB, provided that the array was nonuniformly excited by a proper tapered amplitude distribution. As for medium scan angles up to 45°, it was demonstrated that dual-mode antenna elements, along with tapered distributions, further facilitated grating lobe reduction as low as -30 dB. The proposed method was also examined for wider scan angles of 50° and 60° in the same phased array configuration with slightly smaller interelement spacing in the order of three quarters of a wavelength. The method was successfully proven to be effective for such wide scan angles, resulting in grating lobes below -22 dB. The full-wave simulation results were also presented, successfully validating the analytical predictions based on the cavity model. The main idea was based on realizing the radiation-matched element patterns for a given scan angle, along with effectively utilizing the self-scanning and nulling properties of such dual-mode antenna elements. The proposed scanning phased array antenna has promising potential for the future generation of phased array antennas with reduced grating lobes beyond the commonly used halfwavelength element spacing. They have numerous applications in wide-angle scanning radars, passive multifunctional imaging radars, massive multi-input multi-output radars, automotive radars such as collision avoidance, intelligent vehicle highway, and autonomous cruise control radars, as well as atmospheric remote sensing, surveillance systems, and many more.

### ACKNOWLEDGMENT

The authors would like to thank the anonymous reviewers for their valuable and constructive comments and suggestions, which certainly improved the clarity and quality of this paper.

#### REFERENCES

- R. J. Mailloux, *Phased Array Antenna Handbook*, 2nd ed. Norwood, MA, USA: Artech House, 2005.
- [2] A. Vosoogh and P.-S. Kildal, "Simple formula for aperture efficiency reduction due to grating lobes in planar phased arrays," *IEEE Trans. Antennas Propag.*, vol. 64, no. 6, pp. 2263–2269, Jun. 2016.
- [3] R. Mailloux and G. Forbes, "An array technique with grating-lobe suppression for limited-scan applications," *IEEE Trans. Antennas Propag.*, vol. AP-21, no. 5, pp. 597–602, Sep. 1973.
- [4] R. Mailloux and A. Martinez, III, "Grating lobe control in limited scan arrays," *IEEE Trans. Antennas Propag.*, vol. AP-27, no. 1, pp. 79–85, Jan. 1979.
- [5] R. F. Harrington, "Sidelobe reduction by nonuniform element spacing," IRE Trans. Antennas Propag., vol. 9, no. 2, pp. 187–192, Mar. 1961.
- [6] V. Bavaro, G. Caliano, and M. Pappalardo, "Element shape design of 2-D CMUT arrays for reducing grating lobes," *IEEE Trans. Ultrason.*, Ferroelectr., Freq. Control, vol. 55, no. 2, pp. 308–318, Feb. 2008.
- [7] H. Wang, D. G. Fang, and Y. L. Chow, "Grating lobe reduction in a phased array of limited scanning," *IEEE Trans. Antennas Propag.*, vol. 56, no. 6, pp. 1581–1586, Jun. 2008.
- [8] W. C. Barott and P. G. Steffes, "Grating lobe reduction in aperiodic linear arrays of physically large antennas," *IEEE Antenna Wireless Propag. Lett.*, vol. 8, pp. 406–408, Sep. 2008.
- [9] M. G. Bray, D. H. Werner, D. W. Boeringer, and D. W. Machuga, "Optimization of thinned aperiodic linear phased arrays using genetic algorithms to reduce grating lobes during scanning," *IEEE Trans. Antennas Propag.*, vol. 50, no. 12, pp. 1732–1742, Dec. 2002.
- [10] D. Blanco, N. Llombart, and E. Rajo-Iglesias, "On the use of leaky wave phased arrays for the reduction of the grating lobe level," *IEEE Trans. Antennas Propag.*, vol. 62, no. 4, pp. 1789–1795, Apr. 2014.
- [11] S. P. Skobelev and P.-S. Kildal, "Blindness removal in arrays of rectangular waveguides using dielectrically loaded hard walls," *IEEE Trans. Antennas Propag.*, vol. 46, no. 4, pp. 546–550, Apr. 1998.
- [12] C. A. Balanis, Antenna Theory: Analysis and Design, 4th ed. Hoboken, NJ, USA: Wiley, 2016.
- [13] Y.-F. Cheng, X. Ding, W. Shao, and B.-Z. Wang, "Planar wide-angle scanning phased array with pattern-reconfigurable windmill-shaped loop elements," *IEEE Trans. Antennas Propag.*, vol. 65, no. 2, pp. 932–936, Feb. 2017.
- [14] Y.-F. Cheng, X. Ding, W. Shao, M.-X. Yu, and B.-Z. Wang, "A novel wide-angle scanning phased array based on dual-mode patternreconfigurable elements," *IEEE Antennas Wireless Propag. Lett.*, vol. 16, pp. 396–399, Jun. 2016.
- [15] X. Ding, Y.-F. Cheng, W. Shao, H. Li, B.-Z. Wang, and D. E. Anagnostou, "A wide-angle scanning planar phased array with pattern reconfigurable magnetic current element," *IEEE Trans. Antennas Propag.*, vol. 65, no. 3, pp. 1434–1439, Mar. 2017.
- [16] A. Pal, A. Mehta, D. Mirshekar-Syahkal, and H. Nakano, "2×2 phased array consisting of square loop antennas for high gain wide angle scanning with low grating lobes," *IEEE Trans. Antennas Propag.*, vol. 65, no. 2, pp. 576–583, Feb. 2017.
- [17] C.-M. Liu, S.-Q. Xiao, H.-L. Tu, and Z. Ding, "Wide-angle scanning low profile phased array antenna based on a novel magnetic dipole," *IEEE Trans. Antennas Propag.*, vol. 65, no. 3, pp. 1151–1162, Mar. 2017.
- [18] Y.-Q. Wen, B.-Z. Wang, and X. Ding, "Wide-beam circularly polarized microstrip magnetic-electric dipole antenna for wide-angle scanning phased array," *IEEE Antennas Wireless Propag. Lett.*, vol. 16, pp. 428–431, Jun. 2016.

- [19] L. Shafai and H. A. Ragheb, "Element reduction in phased arrays using dual-mode self-scanning elements," *Can. J. Elect. Comput. Eng.*, vol. 17, no. 3, pp. 98–106, Jul. 1992.
- [20] J. Huang, "Circularly polarized conical patterns from circular microstrip antennas," *IEEE Trans. Antennas Propag.*, vol. AP-32, no. 9, pp. 991–994, Sep. 1984.
- [21] A. G. Derneryd, "Analysis of the microstrip disk antenna element," *IEEE Trans. Antennas Propag.*, vol. AP-27, no. 5, pp. 660–664, Sep. 1979.
- [22] A. Ludwig, "The definition of cross polarization," *IEEE Trans. Antennas Propag.*, vol. AP-21, no. 1, pp. 116–119, Jan. 1973.
- [23] High Frequency Structure Simulator (HFSS 18.0). Canonsburg, PA, USA, ANSYS, 2017.



**Zabed Iqbal** (S'16) was born in Dhaka, Bangladesh, in 1991. He received the B.Sc. degree in electrical, electronic and communication engineering from the Military Institute of Science and Technology, Dhaka, in 2012, and the M.S. degree in electrical engineering from Georgia Southern University, Statesboro, GA, USA, in 2017. He is currently pursuing the Ph.D. degree in electrical engineering with The University of Alabama in Huntsville, Huntsville, AL, USA.

From 2013 to 2015, he was a Lecturer and a Coordinator with the Department of Electrical and Electronic Engineering, Z. H. Sikder University of Science and Technology, Shariatpur, Bangladesh. His current research interests include antennas, phased array radars, and electromagnetics.



Maria Pour (S'06–M'11–SM'16) received the B.Sc. degree in electrical engineering from the Sharif University of Technology, Tehran, Iran, in 1997, and the M.Sc. and Ph.D. degrees in electrical engineering from the University of Manitoba, Winnipeg, MB, Canada, in 2006 and 2012, respectively.

She was a Research Associate and the Assistant Director with the Antenna Laboratory, University of Manitoba. In 2015, she joined the Department of Electrical and Computer Engineering, The University of Alabama in Huntsville, Huntsville, AL, USA,

as an Assistant Professor. She has co-authored six book chapters and has authored over 60 journal papers and conference proceedings. Her current research interests include the areas of antennas, applied electromagnetics, remote sensing, antenna theory, design, and analysis, including reflector antennas and feeds, primary matched feeds, phased array antennas, virtual aperture antennas, multimode antennas, dual-polarized dual-band antennas, and antenna measurement techniques.

Dr. Pour received the 2017 CAREER Award from the U.S. National Science Foundation. She is named as the 2017 Outstanding Junior Faculty and the 2017 Outstanding Research Faculty by the College of Engineering, University of Alabama in Huntsville. Since 2016, she has been serving as an Associate Editor for the IEEE TRANSACTIONS ON ANTENNAS AND PROPAGATION.